Status Update: Deposition Modeling For SNF Canister CISCC

Spent Fuel and Waste Disposition

Prepared for
U.S. Department of Energy
Spent Fuel and Waste Science and Technology
Philip Jensen
Sarah Suffield
Ben Jensen
Pacific Northwest National Laboratory

December 18, 2020
M3SF-21PN010207025
M3SF-20PN0102070412
PNNL-30793

DISCLAIMER

This information was prepared as an account of work sponsored by an agency of the U.S. Government. Neither the U.S. Government nor any agency thereof, nor any of their employees, makes any warranty, expressed or implied, or assumes any legal liability or responsibility for the accuracy, completeness, or usefulness, of any information, apparatus, product, or process disclosed, or represents that its use would not infringe privately owned rights. References herein to any specific commercial product, process, or service by trade name, trade mark, manufacturer, or otherwise, does not necessarily constitute or imply its endorsement, recommendation, or favoring by the U.S. Government or any agency thereof. The views and opinions of authors expressed herein do not necessarily state or reflect those of the U.S. Government or any agency thereof.

SUMMARY

This report fulfills the M3 milestones M3SF-21PN010207025 & M3SF-20PN0102070412. During fiscal year (FY) 2020, Pacific Northwest National Laboratory (PNNL) worked to further develop the FY 2019 deposition and particle tracking models. This status report outlines these efforts and presents the progress made so far. Model development work is ongoing and is planned to continue in FY 2021.

The FY 2020 model development included work on:

- Wind Effects. Initial model development and sensitivity studies investigated how wind direction and speed affect deposition.
- Brownian Motion. Implementing Brownian Motion into existing models.
- Particle Size Variability. Depending on the particle composition, the diameter of the particle may vary with changes in relative humidity. Models were developed to analyze this.
- Multiphase and Fluid Film Modeling. Investigating canister surface wetting and drying, and how this effects overall deposition. Models were developed to analyze this.
- Diffusiophoresis. Performing initial work to implement diffusiophoresis into the existing models.
- Turbophoresis. Performing initial work to implement turbophoresis into the existing models.

Much of this work will continue into FY21. The authors present initial results and discuss current and future work.

This page is intentionally left blank.

ACKNOWLEDGEMENTS

The authors would like to thank our U.S. Department of Energy sponsor, Ned Larson, for funding and supporting this work. We would also like to thank our collaborators at Sandia National Laboratories.

This page is intentionally left blank.

CONTENTS

SUMMARY iii

ACKNOWLEDGEMENTS v

ACRONYMS xi

1. INTRODUCTION 1
   1.1 Model Limitations and Disclaimer 1

2. BACKGROUND AND DISCUSSION 3

3. DEPOSITION MODEL DEVELOPMENT 5
   3.1 Wind Effects 5
      3.1.1 Model Development 5
      3.1.2 Results 11
   3.2 Brownian Motion 17
   3.3 Multiphase and Particle Size Variability 20
   3.4 Multiphase and Fluid Film 25
   3.5 Diffusiophoresis 26
   3.6 Turbophoresis 27

4. FUTURE WORK 31

5. CONCLUSION 33

6. REFERENCES 35

This page is intentionally left blank.

LIST OF FIGURES

Figure 3-1. HSMH-15 external fluid region dimensions 6
Figure 3-2. External fluid region mesh for the 90-degree wind direction case 7
Figure 3-3. 35 kW – External Fluid Model – Wind 0 m/s 8
Figure 3-4. 35 kW – Original Model 9
Figure 3-5. Fluid velocity magnitude for wind profile $v10 = 5$ m/s, 0 degree, and 35kW heat load 10
Figure 3-6. HSM Inlet and Outlet Naming Convention 11
Figure 3-7: Preliminary: 35kW 5 m/s at 0 degrees side view external wind vector 17
Figure 3-8: Preliminary: 35kW 5 m/s at 0 degrees top view external wind vector 17
Figure 3-9. Overall deposition for HSM-15 model with a 35-kW heat load after 20 seconds for no user defined particle forces (no Brownian or thermophoretic forces) in the top image and with a user-defined Brownian particle force in the bottom image. 19
Figure 3-10. Particle velocity in the axial canister direction for HSM-15 model with a 35-kW heat load after 20 seconds for no user defined particle forces (no Brownian or thermophoretic forces) in the top image and with a user defined Brownian particle force in the bottom image. 20
Figure 3-11. HSM-15 model with a 35-kW heat load and 80 percent RH showing canister surface temperatures (top) and canister surface RH (bottom). 21
Figure 3-12. Droplet evaporation from the Davies et al. (2012) experiment (left) and from the STAR-CCM+ simple model (right). 22
Figure 3-13. Canister deposition MAGNASTOR model with a 35-kW heat load and 80 percent RH for no droplet evaporation (top) and droplet evaporation (bottom). 23
Figure 3-14. Canister deposition HSM-15 model 35-kW heat load and 80 percent RH with no droplet evaporation (top) and droplet evaporation (bottom) 24
Figure 3-15. Canister deposition HSM-15 model 5-kW heat load and 80 percent RH with no droplet evaporation (top) and droplet evaporation (bottom) 25
Figure 3-16. HSM-15 fluid film model film mass. 26
Figure 3-17. Canister deposition for vertical MAGNASTOR model with 35-kW heat load for no turbulent dispersion (top) and with turbulent dispersion (bottom). 28
Figure 3-18. Canister deposition for horizontal HSM-15 model with 35-kW heat load for no turbulent dispersion (top) and with turbulent dispersion (bottom). 29

LIST OF TABLES

Table 3-1. Key statistics comparing the external fluid and original model 8
Table 3-2. Preliminary: 35kW – Inlet and Outlet Flow Rates 13
Table 3-3. Preliminary: 5kW – Inlet and Outlet Flow Rates 14
Table 3-4. Preliminary: 35kW Wind Effects Deposition Results 15
Table 3-5. Preliminary: 5kW Wind Effects Deposition Results 16

ACRONYMS

CDF	cumulative distribution function
CISCC	chloride-induced stress corrosion cracking
DCS	dry cask simulator
DSC	dry shielded canister
FY	fiscal year
HSM	horizontal storage module
ISFSI	independent spent fuel storage installation
NRC	U.S. Nuclear Regulatory Commission
PNNL	Pacific Northwest National Laboratory
RH	relative humidity
SNF	spent nuclear fuel
SNL	Sandia National Laboratories
SSA	sea salt aerosol

This page is intentionally left blank.

STATUS UPDATE: DEPOSITION MODELING FOR SNF CANISTER CISCC

1. INTRODUCTION

This report describes further development of the deposition models presented in fiscal year (FY) 2019 in the milestone report, *Preliminary Deposition Modeling: For Determining the Deposition of Corrosive Contaminants on SNF Canisters* (Jensen et al. 2020). The preliminary work, presented in FY 2019, focused on the initial development of deposition models. The FY 2020 work presented herein focused on further developing the models. This includes further investigation into boundary conditions, particle size, and deposition mechanisms. These investigations focused on best approaches for implementing these effects into the existing Pacific Northwest National Laboratory (PNNL) deposition and thermal models, modeling best practices, and investigations into the importance of various deposition mechanisms. This report is a status report, initial results are presented, and a thorough discussion of future work is included.

1.1 Model Limitations and Disclaimer

The modeling results shown herein are preliminary and for information only. The models are useful for understanding the physics of particle tracking and deposition as it applies to spent nuclear fuel (SNF) canisters. However, they are not the final analysis of the systems discussed herein, and additional model development and testing will be needed before models such as these can be useful for determining the likelihood of chloride-induced stress corrosion cracking (CISCC) on SNF canisters.

While the PNNL thermal models are well developed, the deposition models are preliminary and will require further development.

The deposition models, deposition results, and the deposition modeling methodology described in this report are not verified and validated. Detailed and thorough testing is required to verify and validate these models. Such testing is required before deposition modeling such as this can be used to predict actual deposition on deployed canisters at independent spent fuel storage installation (ISFSI) sites.

This page is intentionally left blank.

2. BACKGROUND AND DISCUSSION

Nuclear power plants produce SNF, which is considered radioactive waste under current U.S. policy. It is possible that SNF will be stored at the reactor site or consolidated interim storage facilities for periods longer than a century. The U.S. Nuclear Regulatory Commission (NRC) has concluded that SNF generated by any reactor can be safely stored for 60 years beyond the licensed life of a reactor. Furthermore, it has been acknowledged that for long-term storage of up to 160 years beyond the licensed life of the reactor, "one time replacement of the ISFSIs and spent fuel canisters and cask" may be required (NRC 2014). At present, the technical basis is insufficient to support long-term storage without the replacement of the spent fuel canisters. In addition, without future policy action, one must assume and plan for extended SNF storage at ISFSI locations.

During dry storage, the primary canister degradation process is likely to be CISCC at the heat-affected zones of the canister welds (NRC 2012). While it is currently unknown if there is a threshold concentration for CISCC initiation, one can assume that the onset and progress of material degradation will depend on local contaminant concentration, the properties of the contaminant species, and synergistic effects when multiple contaminants are present. The primary contaminant of concern is chloride, which is dispersed in the atmosphere and then deposits on to the canisters. Currently, the rate of chloride deposition onto the canisters is unknown. Modeling is being developed that will aid in filling this knowledge gap.

Previous deposition modeling work focused on investigating the feasibility of modeling and identifying key phenomena to include in the models. The FY 2019 deposition modeling successfully demonstrated that modeling could be used to determine the rate of deposition onto canister surfaces. The FY 2019 modeling included implementing particle tracking into the existing PNNL thermal models and the integration of one phoretic deposition mechanism into the models. This was demonstrated for the Sandia National Laboratories (SNL) dry cask simulator (DCS), the MAGNASTOR®[a] for a vertical system, and the NUHOMS®[b] for a horizontal system. However, these models are preliminary because they were limited in scope. They had a static boundary condition because forced flow was not considered (i.e., no wind), and only one phoretic deposition mechanism was included. Deployed canisters vary widely in design and are subjected to a wide variety of atmospheric conditions. Because of this variability, deeper investigation into various modeling options is necessary. The goal of these investigations is to ascertain which deposition mechanisms are of high importance and to study how changes in boundary conditions affect overall deposition. To this end, PNNL is further developing the models to investigate these effects.

[a] MAGNASTOR® is a registered trademark of NAC International, Peachtree Corners, Georgia

[b] NUHOMS® is a registered trademark of TN Americas LLC (Orano TN).

This page is intentionally left blank.

3. DEPOSITION MODEL DEVELOPMENT

The FY 2020 modeling was focused on further developing the preliminary FY 2019 deposition models (Jensen et al. 2020). These efforts were focused in two areas:

- Wind Effects Deposition Modeling. Wind effects were examined using the existing models and assumptions and applying them to a case that more closely represents a canister located at an ISFSI.
- Additional Deposition Phenomenon. The authors studied which deposition mechanisms are of high importance to the problem of canister CISCC.

Both of these areas represent continuing work, and the information presented herein should be considered a preliminary first step.

3.1 Wind Effects

An ambient wind effects model was developed to better understand how ISFSI metrological conditions affect the deposition of particles on the SNF canisters and inside the overpack. The wind effects modeling calculated the deposition at different windspeeds, wind direction, and heat loads. Four windspeeds at 2.5 m/s, 5 m/s, 15 m/s, and 26.5 m/s at directions varying in 30 degree increments from 0 degrees to 180 degrees at 35kW and 5kW heat loads were analyzed. The 0 degree wind direction is perpendicular to the inlet of the Horizontal Storage Module (HSM). These wind speed cases were analyzed on a NUHOMS HSM-15 (HSM-15) at a heat load of 5kW and 35kW for all direction cases. Future work will investigate wind effects for a vertical system. The wind effects model required additional model development, which is also outlined. The work described in this report is the first attempt at incorporating wind effects into the canister deposition models. Further development, sensitivity studies, and testing are required to verify and validate these models. The results have not been verified and validated.

3.1.1 Model Development

For the wind effects particle deposition modeling study, a STAR-CCM+ thermal model of an HSM-15 was modified. This base model has been developed previously (Suffield et al. 2012; Jensen et al. 2020) and modified for this application by adding an external fluid region around the HSM. The interfaces and boundary conditions were updated to properly represent the HSM sitting in ambient air. To improve computational efficiency, the fuel region and inner details of the canister were removed and replaced with the corresponding heat flux for the specified heat. These heat fluxes were produced using the original model with the fuel region intact.

3.1.1.1 External Ambient Wind Boundary

The external fluid was developed following the main points of best practices for External Aerodynamics outlined in the STAR-CCM+ manual (Siemens 2020). The dimensions of the external fluid region are shown in Figure 3-1. A square box was used because the external wind will be rotated 180 degrees around the HSM. Using the same length and width dimensions enables the particles to be injected at the same distance from the HSM.

This large external fluid boundary is used to minimize effects from the boundaries. For the cases where flow is normal to the HSM (at 0, 90, and 180 degrees), a velocity inlet with downstream outlet was configured. The sides are configured as symmetry boundaries. For the off-normal wind directions, two adjacent sides were set as velocity inlets and the other two adjacent sides were configured to be the pressure outlets. This allowed the wind to flow through the external fluid region to mimic an infinite boundary. For all cases, the top was set as a symmetry boundary. The ambient temperature of the external fluid region is 20°C.

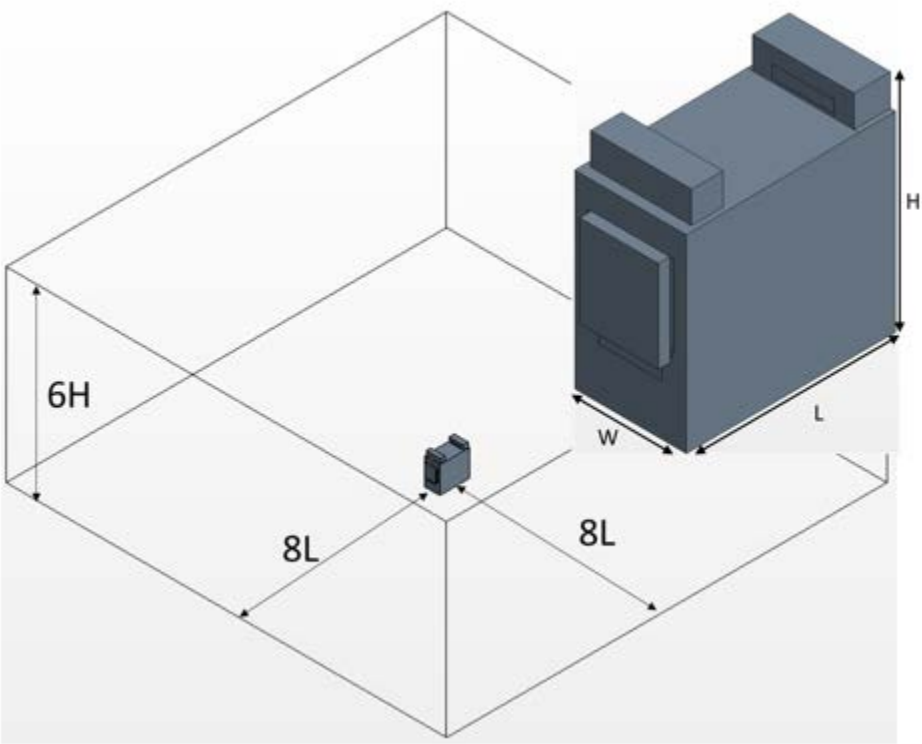

Figure 3-1. HSMH-15 external fluid region dimensions

3.1.1.2 Mesh

Figure 3-2 shows the mesh for the external fluid region. A very course mesh size (~3 m) was chosen for the external fluid boundary. The authors chose this size to increase computational efficiency and keep run times reasonable. The mesh for the HSM and fluid is significantly more refined to capture the detail of those smaller parts. The external fluid region has 49,212 cells and the HSM region has 2,007,768 cells for a total of 2,056,980 cells in the entire model. The small number of cells composing the external fluid region adds little computational expense over the original model. For this study, computational expense was a priority to enable a large number of wind-speed and direction cases. For future detailed studies, the authors will perform a mesh sensitivity study to quantify the effect of this rather course mesh.

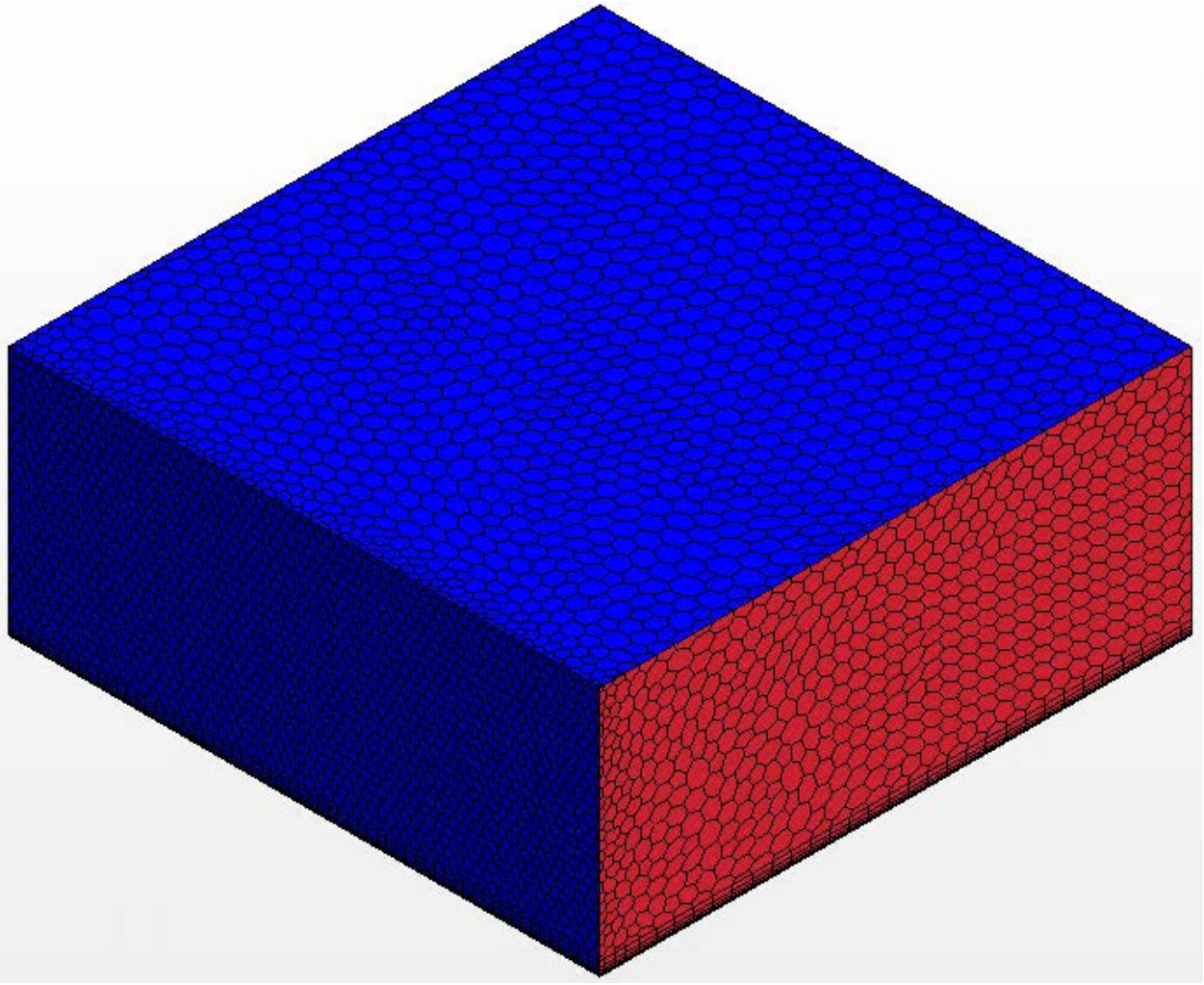

Figure 3-2. External fluid region mesh for the 90-degree wind direction case

3.1.1.3 Stagnant Comparison to Original Model

Table 3-1 shows the comparison of key model results between the original model and the model with the external fluid region. The results of these two models are very similar, which indicates that the external fluid model agrees well with the previous model (Jensen et al. 2020) from which this external fluid model was built. There is a slight difference in the external concrete temperature, this is due to the application of the external boundary which was not present in the previous modeling. Previous modeling used purpose-built heat transfer coefficients at the surface of the HSM. Future work is planned to investigate the application of external boundaries to SNF thermal and deposition models.

One feature that has been omitted from both models is external solar radiation. With the addition of the external fluid region, the definition of solar radiation is different in STAR-CCM+. Adding external solar radiation is left for future investigation.

Figure 3-3 and Figure 3-4 compare the fluid flow for axial cross sections of the external fluid model and original model. Looking at these axial profiles, they seemed to compare well with each other, which provided further information on the validity of the external fluid region model.

Table 3-1. Key statistics comparing the external fluid and original model

Model	Flow into HSM [kg/s]	Flow Out of HSM [kg/s]	Max DSC Temp [°C]	Avg DSC Temp [°C]	Max Concrete Temp [°C]	Avg Concrete Temp [°C]
Original HSM15	6.03e-01	-6.03e-01	314.29	155.98	141.02	35.88
External Fluid HSM15	5.85e-01	-5.87e-01	312.79	155.88	103.55	37.89

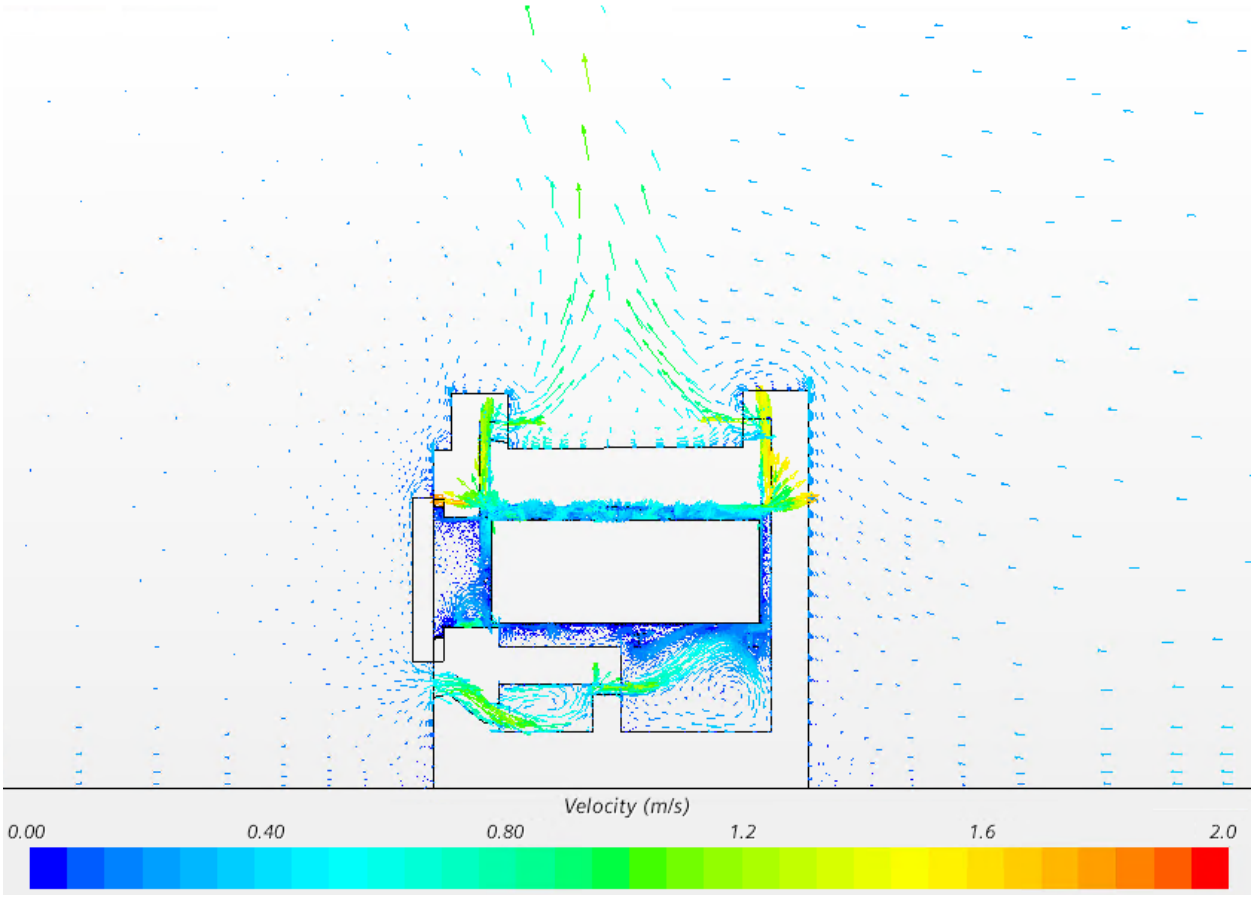

Figure 3-3. 35 kW – External Fluid Model – Wind 0 m/s

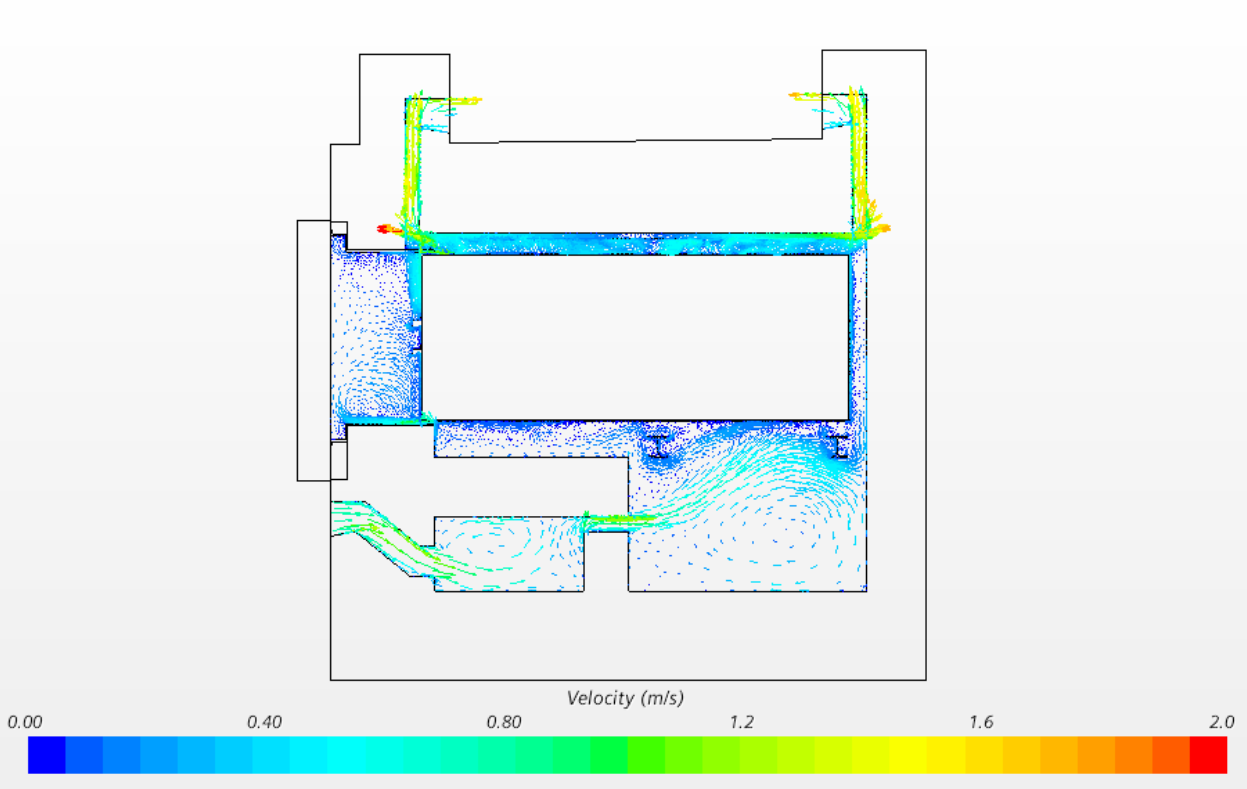

Figure 3-4. 35 kW – Original Model

3.1.1.4 Wind Profile – 10m

To account for surface features surrounding the HSM (terrain, buildings, cars, and anything else that obstructs wind flow), an elevation-varying wind velocity profile was used. For common engineering applications such as this, a power-varying wind profile is recommended by Hsu et al. (1994).

$$v = v_{10}\left(\frac{z}{z_{10}}\right)^{1/7}$$

The windspeed is assumed to vary from ground level (0 meters) to 10 meters in elevation, so $z_{10} = 10\ m$. v_{10} is the constant wind velocity above 10 meters. v is the velocity at z meters of elevation above the ground.

The resulting wind velocity profile for a constant wind speed of $v_{10} = 5$ m/s is applied at the boundary, and the results are shown in Figure 3-5.

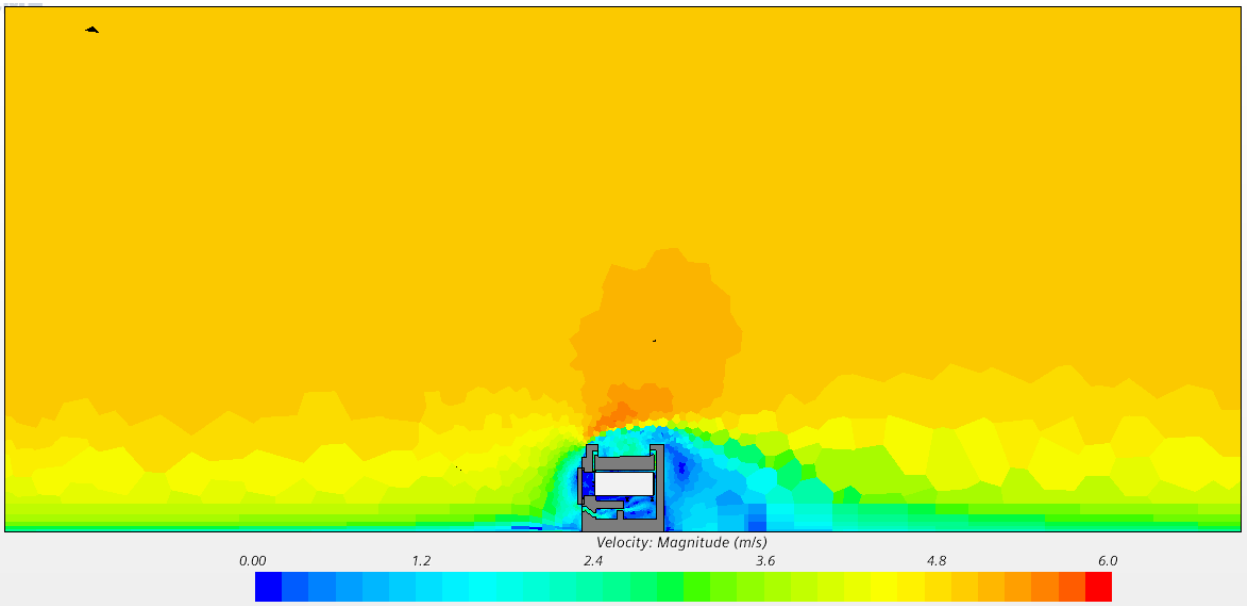

Figure 3-5. Fluid velocity magnitude for wind profile $v_{10} = 5$ m/s, 0 degree, and 35kW heat load

3.1.1.5 Windspeed and Direction

The authors analyzed wind speeds at 2.5 m/s, 5 m/s, 15 m/s, and 26.5 m/s. For each of these wind speeds, the wind direction was varied at 30 degree increments. The wind directions started perpendicular to the inlet of the HSM at 0 degrees and moved around to 180 degrees, perpendicular to the back of the HSM.

The windspeed and direction modeling indicates that flow across the inlet and outlets can vary as wind direction changes. In some instances, the flow at an outlet can be reversed. The naming convention for the windspeed and direction modeling is shown in Figure 3-6, and the results for high and low decay heat rates are shown in Table 3-2 and Table 3-3. These models were developed to investigate how windspeed and direction may affect deposition rates. As such, analyzing the canister and fuel thermal performance is outside the scope of this study. In some cases, the difference between the mass flow rate at the inlets and outlets yields a non-zero result. This can be attributed to numerical error, but in some instances the difference was deemed sufficiently large to warrant further discussion. It is important to remember that these results are preliminary and may vary as the models are refined and further developed. Therefore, results that exceeded a difference of +/- 0.03 kg/s are not reported. The modeling of wind effects as it is applied to SNF canisters is complex and demonstrates the need for standalone wind effects modeling in the future.

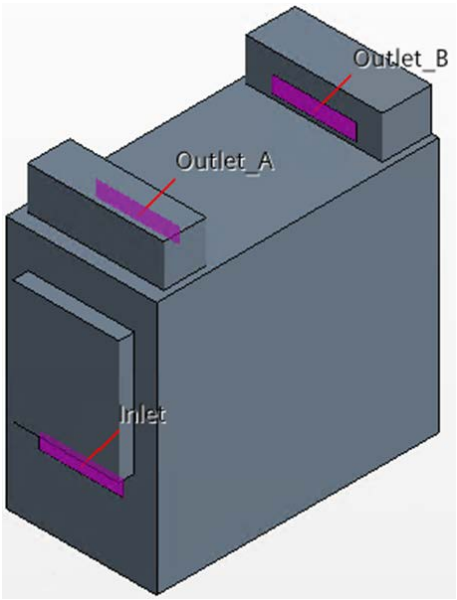

Figure 3-6. HSM Inlet and Outlet Naming Convention

3.1.1.6 Particle Injectors

The particle injector points are important to modeling ambient particles. In STAR-CCM+, particles are injected at discrete points on parts or part boundaries. In real life these particles are most likely well mixed with the ambient air. To explore different particle injection strategies and attempting to model fully mixed particles, the authors investigated different particle injection strategies. This was an important step, and all future studies will need to perform a sensitivity study to determine the best particle injection strategy. For this study PNNL investigated several injector grid sizes and placements within the modeling domain. A 101 x 101 injector grid, placed 45.5 m away from the center of the HSM, yielded the best balance between modeling resolution and computational performance. When changing the wind direction, the injection grid was rotated about the center of the HSM to remain perpendicular to the wind direction of interest. Future studies will be necessary to determine appropriate guidelines for particle injection into canister deposition models.

3.1.2 Results

Table 3-4 and Table 3-5 show the particle deposition results for the wind speed, direction, and heat loads cases analyzed in this modeling effort. These results are presented as deposition efficiencies, (i.e., the percentage of particles that were assumed to adhere to a surface of interest). Results are presented for the external surfaces of the HSM, internal surfaces of the HSM, the total for the HSM, the canister, and the total system deposition efficiency. The results indicate that only a small percentage of what is injected at the boundary deposits on the canister. These models assume that the only source of particles is at the boundary, once a particle leaves the boundary it cannot reenter, and no particles are generated in the modeling domain.

This model used the FY 2019 HSM and canister deposition models (Jensen et al 2020). These models are limited in that only aerodynamic and gravitational deposition is considered. The only phoretic mechanism present is the thermophoretic force. No resuspension of deposited particles is considered. A uniform particle size distribution with a range of 0.25-25 μm was used. These models have not been verified or validated. Therefor these modeling results should be considered preliminary.

Figure 3-7 and Figure 3-8 show the vector fields of the external wind surrounding the HSM for one windspeed and direction. These figures demonstrate how wind may affect the overall deposition. A stagnation area can be seen at the front of the HSM, the air then interacts with this area and flows around the HSM. The air being redirected around the face of the HSM contributes to lower particle deposition efficiency on those frontal surfaces directly incident to the wind, and lower particle count entering the HSM inlet.

Table 3-2. Preliminary: 35kW – Inlet and Outlet Flow Rates

Case	Max DSC Temp [°C]	Avg DSC Temp [°C]	Mass Air Flow Inlet [kg/s]	Mass Air Flow Outlet A [kg/s]	Mass Air Flow Outlet B [kg/s]
2.5m/s 0 deg	304.34	147.64	0.87	-0.36	-0.51
2.5m/s 30 deg	312.35	149.95	0.76	-0.39	-0.37
2.5m/s 60 deg	307.26	151.30	0.64	-0.30	-0.33
2.5m/s 90 deg	312.71	153.11	0.57	-0.25	-0.32
2.5m/s 120 deg	308.01	152.84	0.61	-0.22	-0.39
2.5m/s 150 deg	299.64	153.91	0.40	0.11	-0.52
2.5m/s 180 deg	307.01	150.87	0.67	-0.30	-0.36
5m/s 0 deg	301.83	142.67	1.42	-0.67	-0.76
5m/s 30deg	303.76	145.00	1.10	-0.70	-0.41
5m/s 60deg	311.00	149.40	0.79	-0.45	-0.36
5m/s 90 deg	311.96	154.47	0.51	-0.22	-0.28
5m/s 120 deg	311.67	150.30	0.75	-0.19	-0.53
5m/s 150 deg	300.07	152.67	0.31	0.39	-0.68
5m/s 180 deg	305.51	148.39	0.81	-0.38	-0.44
15 m/s 0 deg	252.47	108.58	4.22	-1.73	-2.50
15 m/s 30 deg	300.13	124.09	2.83	-2.09	-0.75
15 m/s 60 deg	307.38	133.75	2.01	-1.33	-0.68
15 m/s 90 deg					
15 m/s 120 deg	292.53	138.62	1.42	0.23	-1.67
15 m/s 150 deg					
15 m/s 180 deg	287.22	135.79	1.75	-0.84	-0.92
26.5 m/s 0 deg	230.98	92.46	7.36	-2.96	-4.42
26.5 m/s 30 deg	274.49	106.34	5.01	-3.72	-1.29
26.5 m/s 60 deg	293.03	118.05	3.64	-2.33	-1.29
26.5 m/s 90 deg					
26.5 m/s 120 deg					
26.5 m/s 150 deg					
26.5 m/s 180 deg	273.17	122.41	2.93	-1.41	-1.55

Table 3-3. Preliminary: 5kW – Inlet and Outlet Flow Rates

Case	Max DSC Temp [°C]	Avg DSC Temp [°C]	Mass Air Flow Inlet [kg/s]	Mass Air Flow Outlet A [kg/s]	Mass Air Flow Outlet B [kg/s]
2.5m/s 0 deg	96.85	48.49	0.74	-0.32	-0.41
2.5m/s 30deg	100.08	49.94	0.58	-0.36	-0.20
2.5m/s 60deg	99.79	50.76	0.45	-0.23	-0.19
2.5m/s 90 deg	100.00	52.28	0.33	-0.14	-0.17
2.5m/s 120 deg	100.71	51.09	0.34	0.01	-0.34
2.5m/s 150 deg	86.14	51.01	0.21	0.21	-0.39
2.5m/s 180 deg	96.52	50.33	0.45	-0.19	-0.25
5m/s 0 deg	88.16	46.58	1.39	-0.57	-0.82
5m/s 30deg	97.64	47.54	0.97	-0.70	-0.26
5m/s 60deg	99.48	50.58	0.71	-0.45	-0.26
5m/s 90 deg	102.98	56.00	0.15	0.07	-0.22
5m/s 120 deg	100.77	52.17	0.50	0.05	-0.55
5m/s 150 deg	86.55	51.77	0.14	0.44	-0.60
5m/s 180 deg	95.80	50.61	0.68	-0.31	-0.37
15 m/s 0 deg	63.54	34.05	4.26	-1.74	-2.52
15 m/s 30 deg	91.76	40.57	2.84	-2.12	-0.72
15 m/s 60 deg	96.49	43.37	2.02	-1.37	-0.65
15 m/s 90 deg	83.66	50.05	-0.33	0.44	-0.09
15 m/s 120 deg	82.23	42.32	1.40	0.31	-1.71
15 m/s 150 deg	67.26	37.02	0.31	1.39	-1.69
15 m/s 180 deg	81.57	42.21	1.82	-0.83	-1.00
26.5 m/s 0 deg	53.27	30.37	7.54	-3.09	-4.45
26.5 m/s 30 deg	75.14	34.56	5.05	-3.79	-1.26
26.5 m/s 60 deg	89.22	38.45	3.58	-2.42	-1.17
26.5 m/s 90 deg					
26.5 m/s 120 deg	75.67	37.30	2.48	0.54	-3.02
26.5 m/s 150 deg					
26.5 m/s 180 deg	72.35	36.85	3.34	-1.51	-1.84

Table 3-4. Preliminary: 35kW Wind Effects Deposition Results

Case	External HSM Deposition [%]	Internal HSM Deposition [%]	Total HSM Deposition [%]	Canister Deposition [%]	Total System Deposition [%]
2.5 m/s 0 deg	0.55	0.18	0.73	≤ 0.01	1.46
2.5 m/s 30 deg	0.77	0.17	0.94	≤ 0.01	1.88
2.5 m/s 60 deg	0.86	0.14	1.00	≤ 0.01	2.00
2.5 m/s 90 deg	0.47	≤ 0.01	0.48	≤ 0.01	0.96
2.5 m/s 120 deg	0.65	≤ 0.01	0.66	≤ 0.01	1.32
2.5 m/s 150 deg	0.59	0.06	0.65	≤ 0.01	1.30
2.5 m/s 180 deg	0.37	0.24	0.60	≤ 0.01	1.22
5.0 m/s 0 deg	0.50	0.13	0.63	≤ 0.01	1.27
5.0 m/s 30 deg	0.69	0.12	0.80	≤ 0.01	1.61
5.0 m/s 60 deg	0.88	0.08	0.95	≤ 0.01	1.91
5.0 m/s 90 deg	0.41	≤ 0.01	0.41	≤ 0.01	0.82
5.0 m/s 120 deg	0.64	0.02	0.66	≤ 0.01	1.32
5.0 m/s 150 deg	0.84	0.05	0.89	≤ 0.01	1.78
5.0 m/s 180 deg	0.37	0.03	0.40	≤ 0.01	0.81
15.0 m/s 0 deg	0.52	0.10	0.62	≤ 0.01	1.25
15.0 m/s 30 deg	0.64	0.10	0.74	≤ 0.01	1.48
15.0 m/s 60 deg	0.93	0.06	0.99	≤ 0.01	1.99
15.0 m/s 90 deg					
15.0 m/s 120 deg	0.65	≤ 0.01	0.67	≤ 0.01	1.33
15.0 m/s 150 deg					
15.0 m/s 180 deg	0.40	≤ 0.01	0.41	≤ 0.01	0.82
26.5 m/s 0 deg	0.66	0.14	0.80	≤ 0.01	1.60
26.5 m/s 30 deg	0.67	0.11	0.78	≤ 0.01	1.56
26.5 m/s 60 deg	0.96	0.07	1.02	≤ 0.01	2.05
26.5 m/s 90 deg					
26.5 m/s 120 deg					
26.5 m/s 150 deg					
26.5 m/s 180 deg	0.38	≤ 0.01	0.38	≤ 0.01	0.76

Table 3-5. Preliminary: 5kW Wind Effects Deposition Results

Case	External HSM Deposition [%]	Internal HSM Deposition [%]	Total HSM Deposition [%]	Canister Deposition [%]	Total System Deposition [%]
2.5 m/s 0 deg	0.48	0.18	0.65	≤ 0.01	1.32
2.5 m/s 30 deg	0.78	0.13	0.91	≤ 0.01	1.82
2.5 m/s 60 deg	0.82	0.11	0.93	≤ 0.01	1.86
2.5 m/s 90 deg	0.39	≤ 0.01	0.39	≤ 0.01	0.78
2.5 m/s 120 deg	0.58	≤ 0.01	0.59	≤ 0.01	1.19
2.5 m/s 150 deg	0.56	0.04	0.60	≤ 0.01	1.21
2.5 m/s 180 deg	0.23	0.05	0.28	≤ 0.01	0.57
5.0 m/s 0 deg	0.62	0.11	0.73	≤ 0.01	1.46
5.0 m/s 30 deg	0.67	0.10	0.77	≤ 0.01	1.55
5.0 m/s 60 deg	0.85	0.08	0.93	≤ 0.01	1.87
5.0 m/s 90 deg	0.40	≤ 0.01	0.41	≤ 0.01	0.81
5.0 m/s 120 deg	0.58	0.04	0.62	≤ 0.01	1.24
5.0 m/s 150 deg	0.78	0.03	0.81	≤ 0.01	1.64
5.0 m/s 180 deg	0.43	≤ 0.01	0.44	≤ 0.01	0.89
15.0 m/s 0 deg	0.51	0.10	0.61	≤ 0.01	1.22
15.0 m/s 30 deg	0.64	0.09	0.73	≤ 0.01	1.46
15.0 m/s 60 deg	0.77	0.06	0.83	≤ 0.01	1.66
15.0 m/s 90 deg	0.44	≤ 0.01	0.44	≤ 0.01	0.88
15.0 m/s 120 deg	0.69	0.03	0.72	≤ 0.01	1.44
15.0 m/s 150 deg	0.64	0.05	0.68	≤ 0.01	1.37
15.0 m/s 180 deg	0.40	0.03	0.42	≤ 0.01	0.85
26.5 m/s 0 deg	0.49	0.13	0.62	≤ 0.01	1.24
26.5 m/s 30 deg	0.67	0.09	0.76	≤ 0.01	1.52
26.5 m/s 60 deg	0.76	0.06	0.82	≤ 0.01	1.64
26.5 m/s 90 deg					
26.5 m/s 120 deg	0.67	0.04	0.71	≤ 0.01	1.42
26.5 m/s 150 deg					
26.5 m/s 180 deg	0.38	0.02	0.41	≤ 0.01	0.81

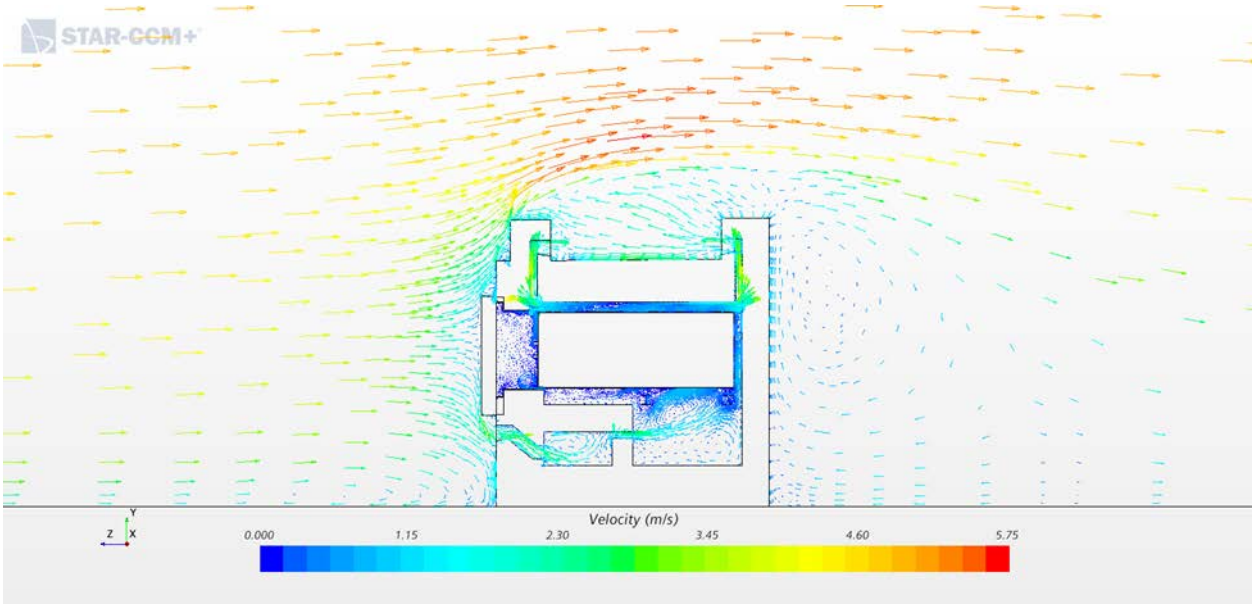

Figure 3-7: Preliminary: 35kW 5 m/s at 0 degrees side view external wind vector

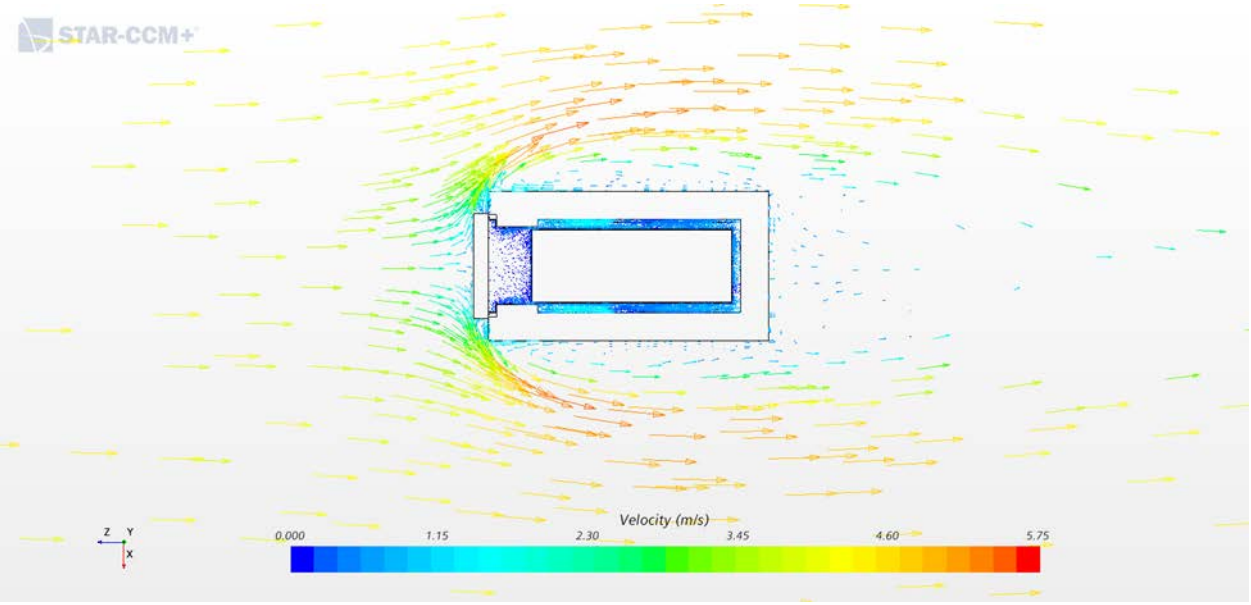

Figure 3-8: Preliminary: 35kW 5 m/s at 0 degrees top view external wind vector

3.2 Brownian Motion

Brownian motion involves the random motion of particles within a carrier fluid resulting from the particles' collision with molecules in the carrier fluid. Brownian particle forces are important for particles with submicron diameters. While most of the mass is expected to be in larger particles. Sub-micron particles could be more abundant but constitute only a tiny fraction of the mass. Brownian motion was implemented into STAR-CCM+ to account for Brownian forces. The equations below were implemented through user defined field functions and a user compiled code (Field 2017). A user compiled code was required to implement a Gaussian random number generator.

$$F_b = \zeta \sqrt{\frac{\pi S_0}{\Delta t}} \quad \text{Eq. 1}$$

$$S_0 = \frac{216 \nu k_B T}{\pi^2 \rho d_p^5 \left(\frac{\rho_p}{\rho}\right)^2 C_c} \quad \text{Eq. 2}$$

$$C_c = 1 + \frac{2\lambda}{d_p}\left(1.257 + 0.4e^{-\left(1.1 d_p / 2\lambda\right)}\right) \quad \text{Eq. 3}$$

Where:
F_b = Brownian force
ζ = a zero mean, unit variance-independent Gaussian random number
Δt = time step
T = absolute temperature of the fluid
ν = kinematic viscosity
k_B = Boltzmann constant
d_p = particle diameter
C_c = Cunningham correction
λ = molecular mean free path

It is important to note that Eq.2 is dependent on the time step, requiring a transient analysis. All models previously developed have been a steady state analysis. The STARCCM+ model of Calvert Cliffs NUHOMS HSM-15 (Jensen et al. 2020) was modified to be a transient analysis that incorporates Brownian forces. The HSM-15 model had incorporated a uniform particle diameter distribution ranging from 0.25-25 um as a cumulative distribution function (CDF) table. Since Brownian forces are expected to be important for particles with submicron diameters, the CDF table was replaced with a constant particle diameter of 0.1 um. The default HSM-15 model also incorporated thermophoresis particle forces.

A series of transient cases were run with the HSM-15 model with different combinations of Brownian and thermophoretic particle forces either turned on or off in the model. For the case with both Brownian and the thermophoretic particle forces accounted for, the two forces are summed together and implemented as a user-defined field function within STAR-CCM+. All cases were initialized with a steady state thermal solution and the Lagrangian solver was frozen during the steady state analysis. Each transient case was run for 20 seconds. An adaptive time-step model was used to set the time step. This adjusted the time step automatically during the run to attain a specified temporal resolution; in this case the time-step size was limited to meet a target Convection Courant, or CFL, number. It took a significant amount of run time to reach 20 seconds, anywhere from 1 to 3 days depending on the computer setup and number of parallel processors used. Future work is recommended to look at reducing the run time of a transient analysis or to look at how the Brownian force equation could be modified to run in a steady state analysis.

The HSM-15 model was run with a heat load of 35 kW and overall deposition plots are shown in Figure 3-9 for two cases: no user-defined particle forces (no Brownian or thermophoretic forces) and with Brownian forces. It is important to note that, with the transient analysis, the authors have more variability from run to run than the previous steady state analysis. In the steady state analysis, the Lagrangian solver is run for one iteration with particles that are injected across the entire inlet surfaces and either deposit on a surface or exit through the outlets. For the transient analysis, particles are injected at the inlet at each time step and track in real time as they migrate through the HSM-15. To significantly reduce solver time,

only a small percentage of injector points are active for each time step, instead of having particles injected at all injector points across the inlet for each time step. The injector points that are active are re-randomized each time step, so that over the course of the transient, all injector points release particles at some point during the analysis. Figure 3-10 shows the particle velocity in the axial canister direction for the no thermophoresis and Brownian case versus the Brownian forces case. The plots show subtle differences in the particle velocity due to the random motion of particles from the Brownian forces. At this time, it is hard to draw any conclusions from the plots due to the limited data set and the unknown variation in transient run variability. The results show the successful integration of Brownian forces into the STAR-CCM+ deposition models and the need for future work in this area.

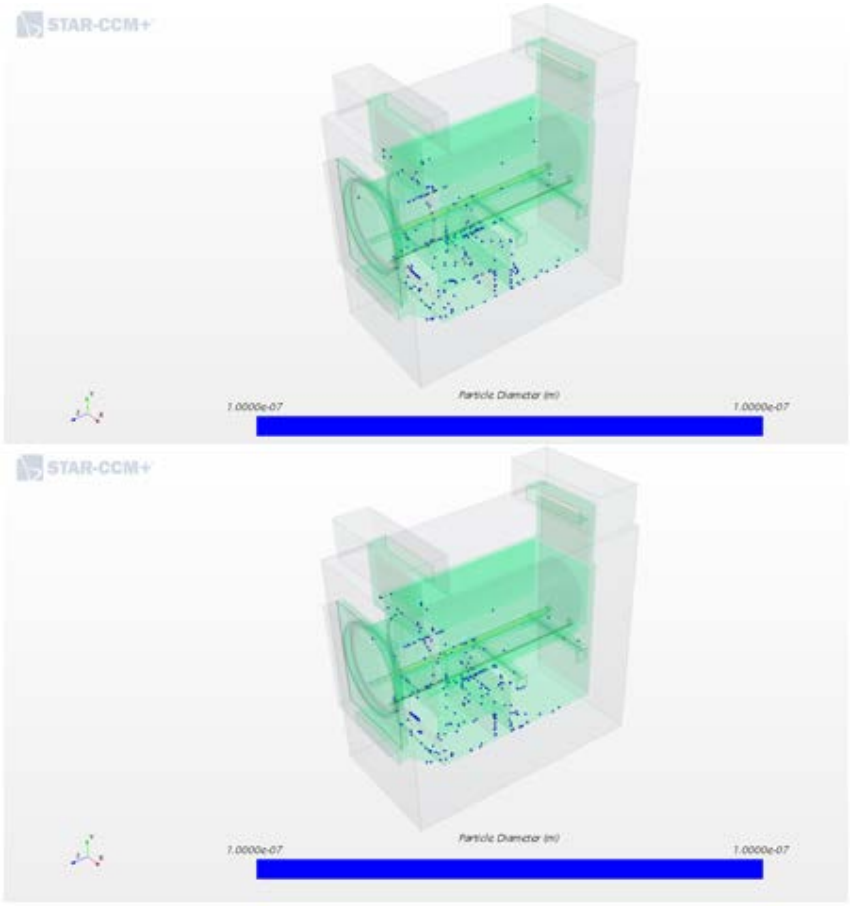

Figure 3-9. Overall deposition for HSM-15 model with a 35-kW heat load after 20 seconds for no user defined particle forces (no Brownian or thermophoretic forces) in the top image and with a user-defined Brownian particle force in the bottom image.

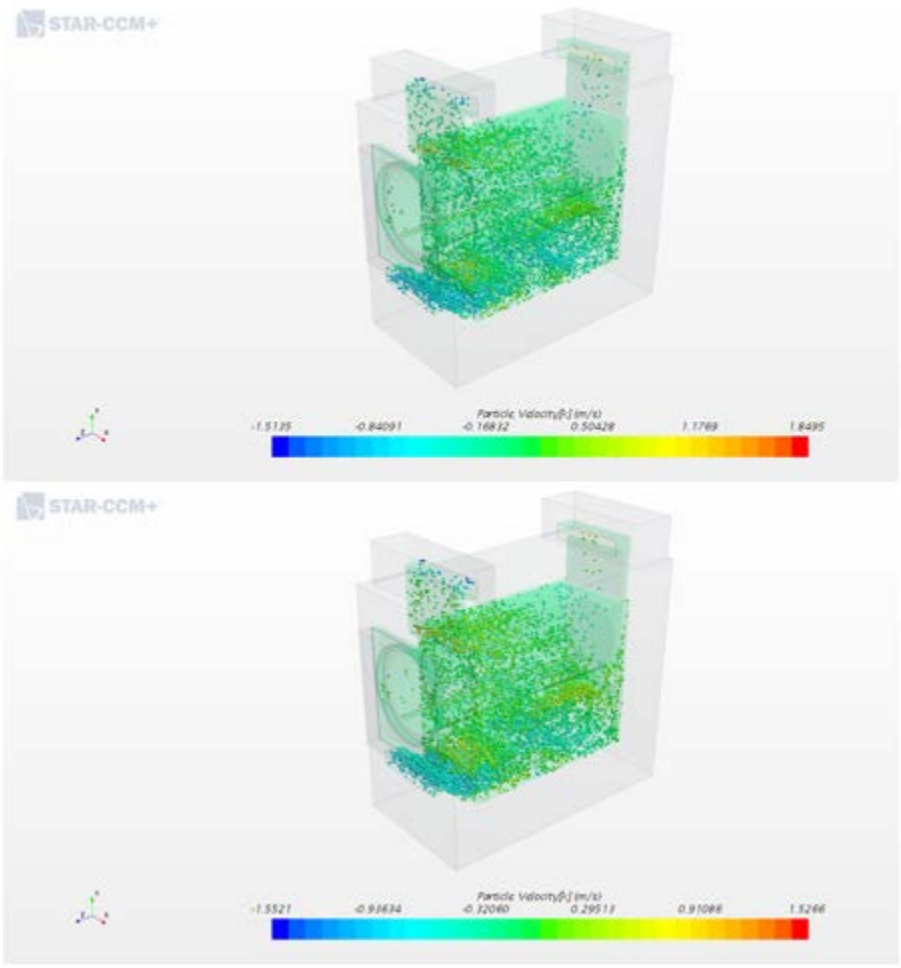

Figure 3-10. Particle velocity in the axial canister direction for HSM-15 model with a 35-kW heat load after 20 seconds for no user defined particle forces (no Brownian or thermophoretic forces) in the top image and with a user defined Brownian particle force in the bottom image.

3.3 Multiphase and Particle Size Variability

The previously developed STAR-CCM+ particle models assumed dry air for the external canister gas. This assumption may not be applicable to canisters deployed at an ISFSI. Some amount of water vapor exists in the air, represented by the relative humidity (RH). Sea salt aerosols (SSAs) are known to change in density as they travel through the atmosphere by responding to changes in RH (i.e., absorbing or shedding water as RH changes). The authors incorporated a multiphase model with air and water vapor accounting for the RH within the air into the STAR-CCM+ particle models. This allowed the models to predict the local RH anywhere in the overpack, including the canister surface. It is assumed that corrosion can occur at any location that is above the deliquescent relative humidity threshold, and the local RH calculations along the canister surface could be used to predict where and when corrosion could occur along the canister surface. The authors modified the HSM-15 model to include a multiphase model with air and water vapor for the environmental gas within the model. Figure 3-11 shows the resulting canister surface temperature and RH plots for a 35-kW heat load and 80 percent RH. The RH plot of the canister surface shows the local values are significantly below the environmental RH of 80 percent.

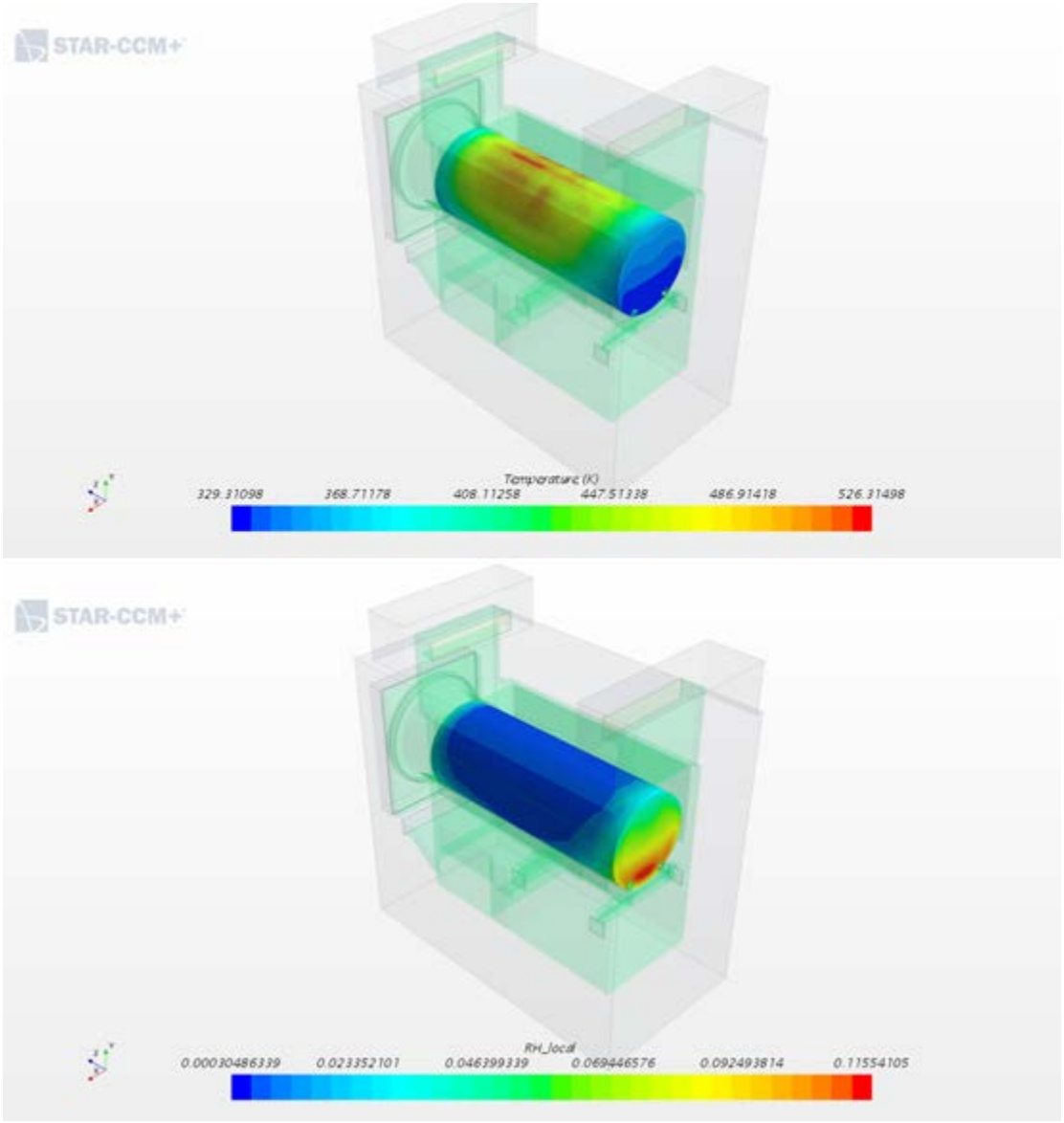

Figure 3-11. HSM-15 model with a 35-kW heat load and 80 percent RH showing canister surface temperatures (top) and canister surface RH (bottom).

A droplet evaporation model was added to the STAR-CCM+ deposition models. The authors set up a series of simple validation models to look at droplet evaporation versus RH before implementing them into the overpack/canister models. A simple droplet model was set up to simulate various experiments and is composed of a static gas region with a droplet injector. The droplets move at a prescribed velocity and temperature to match experimental conditions.

Overall, the STAR-CCM+ model compared well with various experiments found in literature for droplet evaporation. One such experiment was reported in Davies et al. (2012), which presented an evaporation profile for an aqueous sodium chloride droplet in a humid environment. A multicomponent liquid model was used to model the droplet for this STAR-CCM+ model. The multi component liquid was composed of water and NaCl. The relative humidity for the experiment was measured to be 80%. The nitrogen used in Davie et al. (2012) had a low velocity ~ 6 cm/s and an ambient temperature of 20 °C was assumed for the STAR-CCM+ model. The experiment and model results for the droplet evaporation versus time are

shown in Figure 3-12, which compares results between the experiment and STAR-CCM+ model. The authors note that the STAR-CCM+ model and experiment evaporation profiles are in agreement.

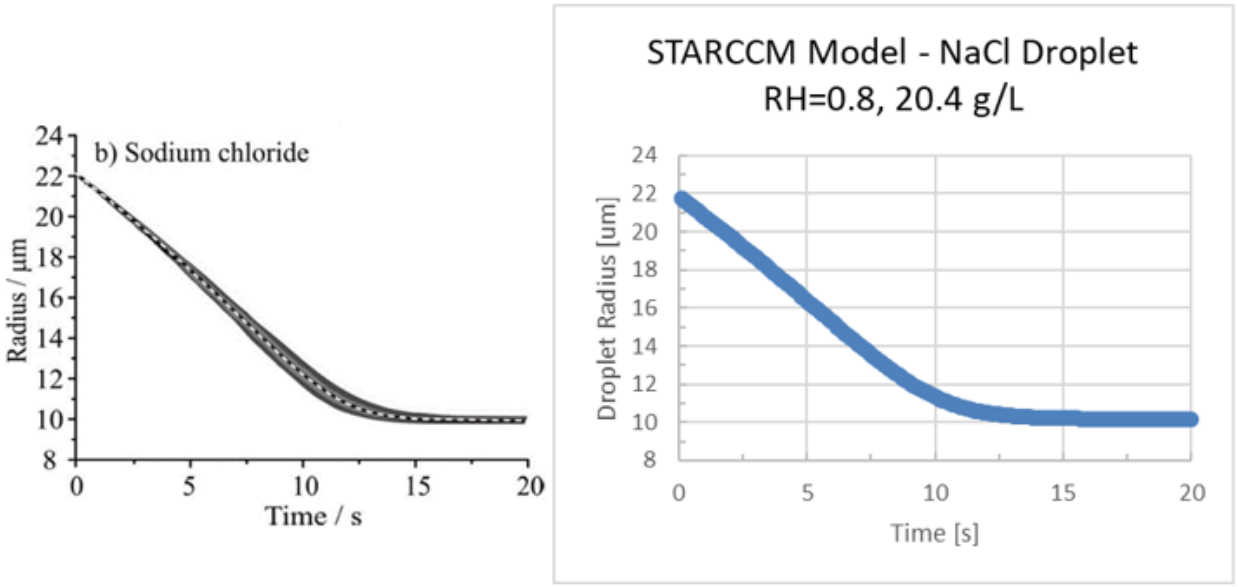

Figure 3-12. Droplet evaporation from the Davies et al. (2012) experiment (left) and from the STAR-CCM+ simple model (right).

The droplet evaporation model was then incorporated into the STAR-CCM+ multiphase models (models with RH accounted for in the environment air) for both the vertical MAGNASTOR system and the horizontal HSM-15 model. Both models were run with 80 percent RH. The authors recommend running the models across a range of RH values in future work. The solid droplet in the initial multiphase model was replaced with a multicomponent liquid representing a SSA particle made up of water and NaCl. Additional work is needed to better understand the particle composition.

The MAGNASTOR model was run at a 35-kW heat load both with and without droplet evaporation. The range of droplet diameters deposited on the canister for each case is shown in Figure 3-13. Additional work is needed to determine how to best measure the deposition on a surface. Previous deposition efficiency results were calculated as a fraction of particle mass on the surface versus total particle mass into the overpack. Since the water within the particle can evaporate, which reduces the particle mass before even impacting a surface, more work is needed to better understand how to evaluate this in the multiphase model.

The high temperatures and flow for the 35-kW case that will contribute to droplet evaporation. The effect can be seen in the range of droplet diameters deposited on the canister between the two cases; the range of particle diameters entering the canister is 2.5e-7 to 2.5e-5 m, the range deposited on the canister for the no-droplet evaporation case. For the case with evaporation droplet, the range is lower, 2.0e-6 to 1.0e-5 m.

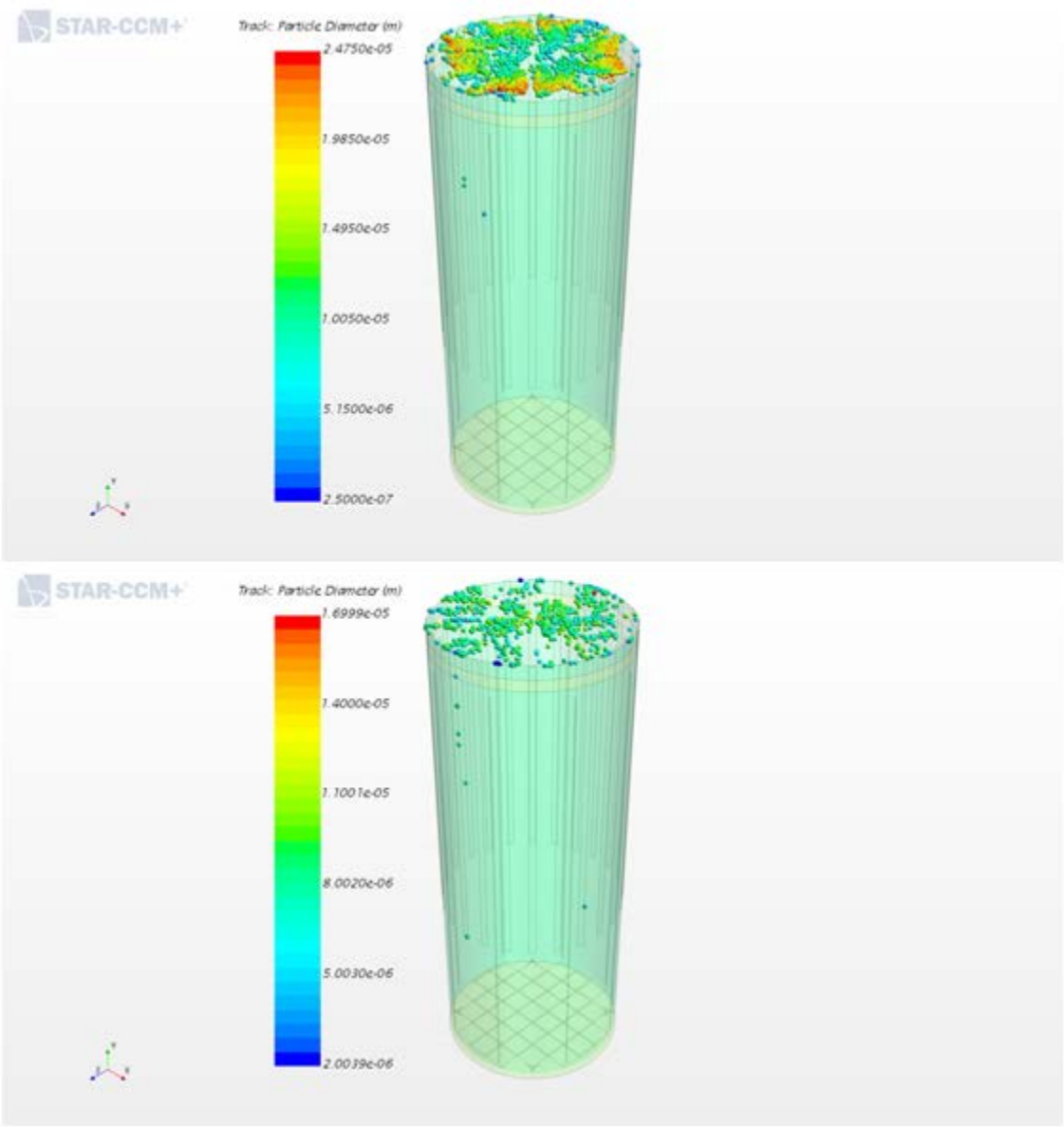

Figure 3-13. Canister deposition MAGNASTOR model with a 35-kW heat load and 80 percent RH for no droplet evaporation (top) and droplet evaporation (bottom).

The HSM-15 model was run at a 5-kW and 35-kW heat load, and each heat load was run both with and without droplet evaporation. Canister deposition and the range of droplet diameters deposited on the canister are shown in Figure 3-14 for the 35-kW cases and shown in Figure 3-15 for the 5-kW cases. The HSM-15 results show similar behavior to the vertical module and that the evaporation of the droplets changes the range of particle diameters that deposit on the canister surface.

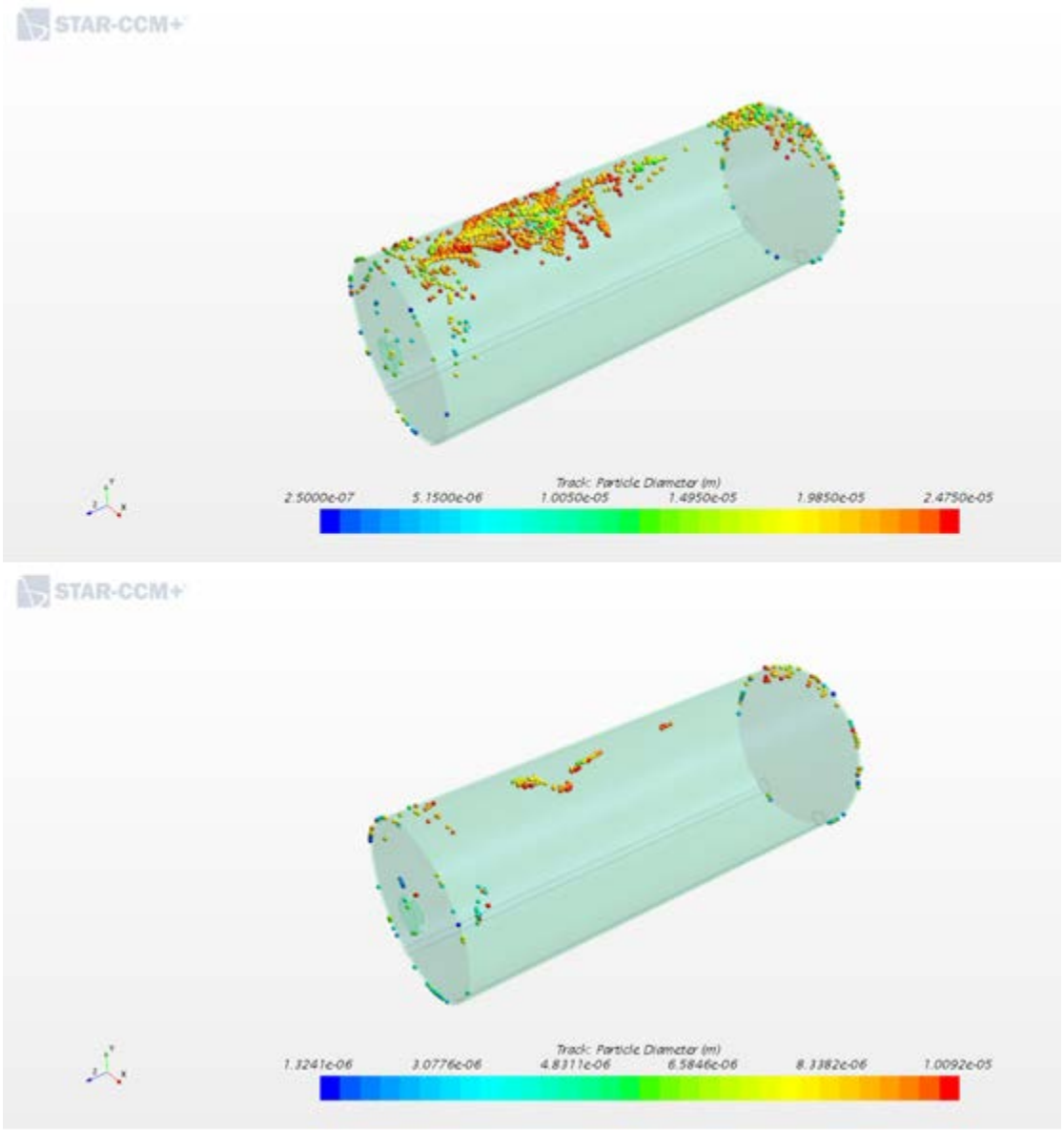

Figure 3-14. Canister deposition HSM-15 model 35-kW heat load and 80 percent RH with no droplet evaporation (top) and droplet evaporation (bottom).

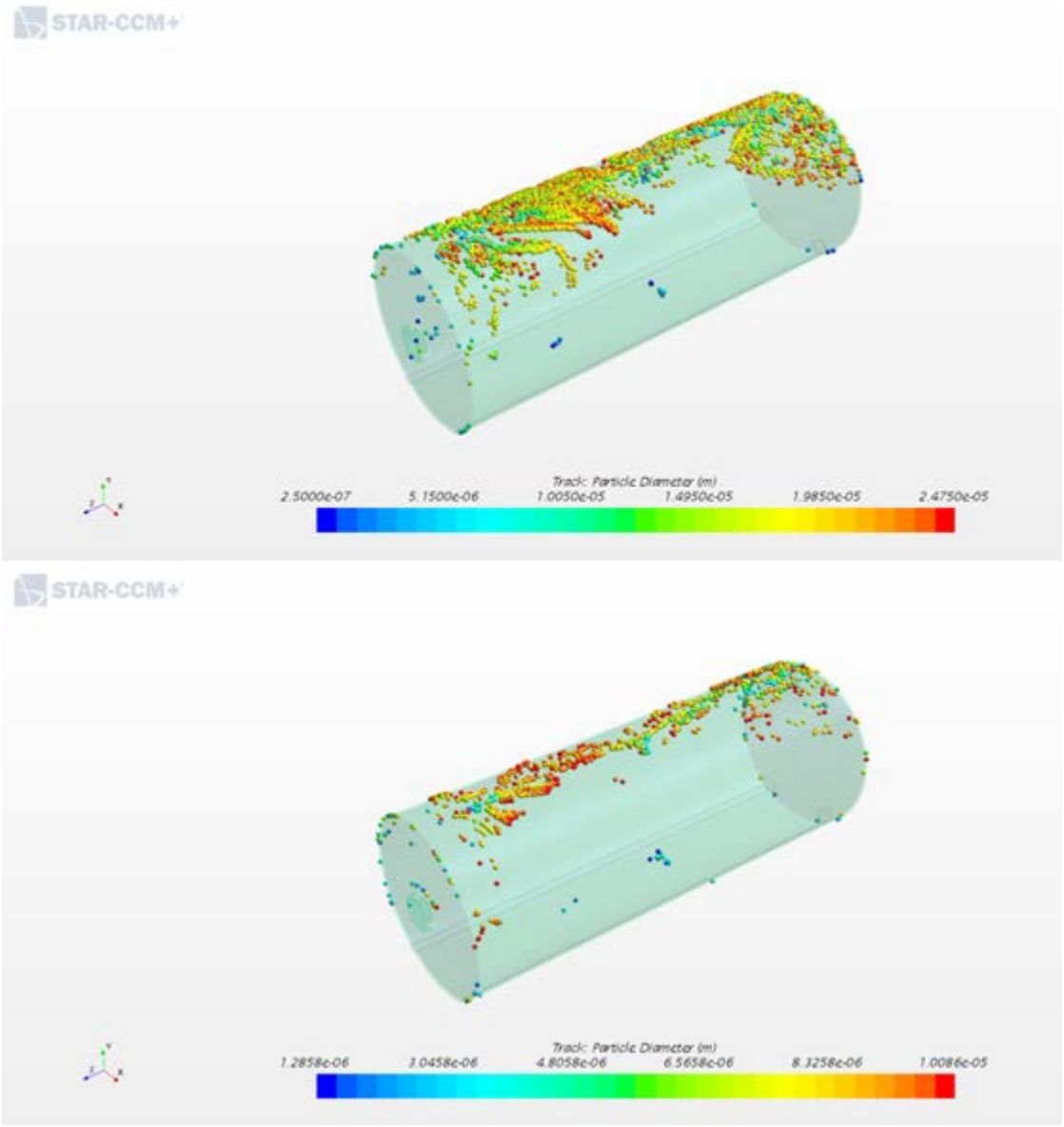

Figure 3-15. Canister deposition HSM-15 model 5-kW heat load and 80 percent RH with no droplet evaporation (top) and droplet evaporation (bottom).

3.4 Multiphase and Fluid Film

The HSM-15 multiphase model was modified to include a fluid film model to look at evaporation or condensation on surfaces within the HSM. The model had to be modified to add evaporation between the fluid film and environment air at surfaces of interest. To do this, a shell interface was created at the heated surface to represent the fluid film. A fluid film was created at the canister surface and along the concrete HSM base. The initial film thickness is set to zero. The fluid film also requires a transient analysis, so the model was modified from a steady to unsteady analysis. For simplicity, no particle flow was included in the fluid film model, but the authors recommend additional future work to incorporate Lagrangian droplets. The HSM-15 fluid film model was initialized with a steady state thermal solution. A heat load of 5-kW was applied within the canister, and an ambient temperature of 35 °C and 95 percent RH was assumed for the transient environment. The model was run out 6 minutes and the resulting fluid film mass

is shown in Figure 3-16. Some condensation occurred along the base of the HSM, but none along the canister surface.

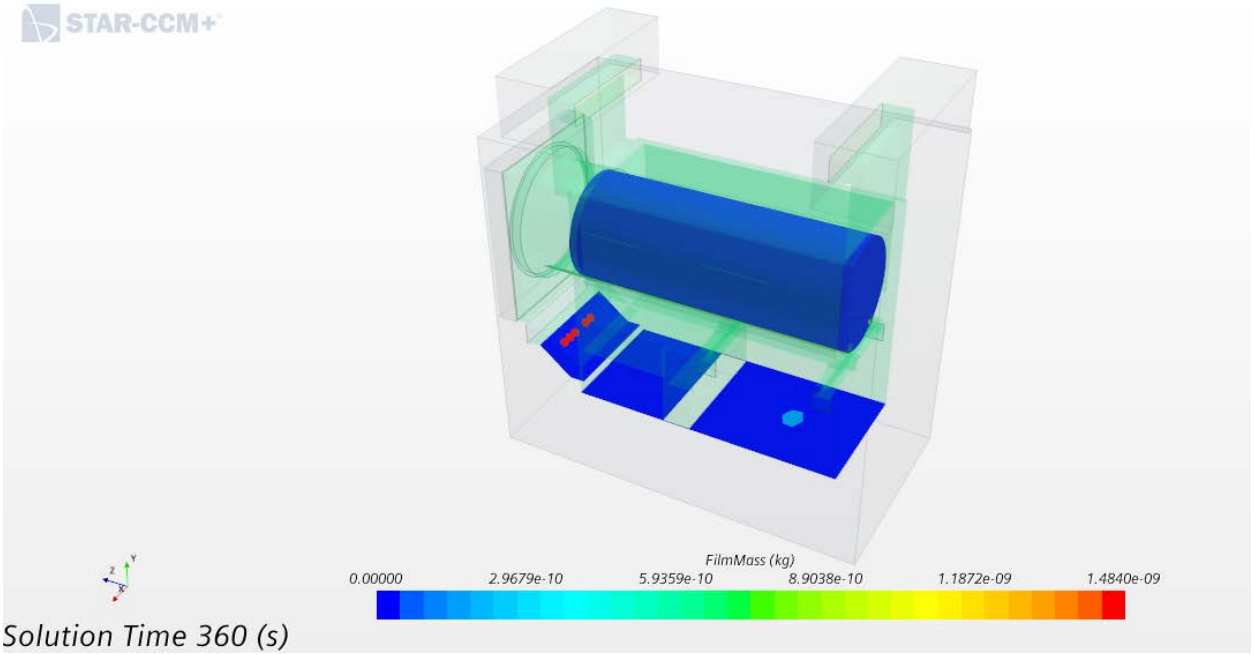

Figure 3-16. HSM-15 fluid film model film mass.

A droplet film transition model could be used in future work to have a fluid film develop once the droplets accumulate to a certain threshold. This threshold is a user-defined setting and determining a representative threshold will be important for implementing a fluid film model in the future. The fluid film model needs further investigation but could be important to implement into the particle deposition model in the future to model the formation of deliquescence surfaces.

These results are preliminary and much more work is needed to develop the fluid film model. A validation problem with condensation should also be looked at in the future to make sure that the fluid film model is capturing the condensation and evaporation physics correctly within STAR-CCM+. The results show an opportunity for an area of further development. Being able to accurately model the evaporation and condensation at a wetted surface could help determine, if an area of the canister surface was to become wet, how long would it take to dry out.

3.5 Diffusiophoresis

Diffusiophoresis is the motion of aerosols caused by a concentration gradient. Since a fluid will naturally try to reach equilibrium, particles will diffuse between two different species of gases. If this diffusion is great enough, any suspended aerosols will experience an external force. In dry storage systems at ISFSIs, diffusiophoresis would potentially be important during conditions in which condensation or evaporation of water vapor occurs. In the case of evaporation of water from a surface, the high concentration of water vapor molecules would diffuse away from the surface, while air molecules would diffuse towards the surface. Aerosols would be expected to be pushed towards the surface due to the heavier mass of air molecules compared to water molecules. In the case of condensation of water onto a surface, aerosols would be expected to be pushed away from the surface because of the low concentration of water vapor molecules near the surface. The authors recommend integrating diffusiophoresis forces into a fluid film model to look at secondary particle effects due to evaporation from a wetted canister surface within the overpack. An approach for implementing diffusiophoresis forces into STAR-CCM+ has been identified,

and an initial simple model has been constructed. The equation for diffusiophoresis force that has been implemented into a STAR-CCM+ as a user-defined force is shown below in Eq. 4 (Pilat and Prem 1976).

$$F_{diff} = \frac{6\pi\mu_g r_p V_D}{C} \quad \text{Eq. 4}$$

Where;
F_{diff} = diffusiophoresis particle force
μ_g = gas viscosity
r_p = particle radius
V_D = particle velocity due to diffusiophoresis
C = Cunningham correction factor

Future work would involve running test cases to compare with experimental data and verify that the diffusiophoresis force is representative in STAR-CCM+.

3.6 Turbophoresis

Turbophoresis is the motion of an aerosol that is caused by differing levels or turbulence. Due to the momentum of surrounding gas particles, an aerosol tends to move from regions of higher turbulence towards regions of lower turbulence. This could result in aerosols moving closer to the canister surface (e.g., into the viscus sublayer) and potentially promote aerosol deposition. To account for turbophoresis in the STAR-CCM+ deposition models, a turbulent dispersion model was added to the Lagrangian model. This turbulent dispersion model was turned on in both the HSM-15 and MAGNASTOR models developed previously (Jensen et al. 2020). No other changes were made to the previous FY 2019 models other than turning on the turbulent dispersion particle model. The models were run for heat loads of 5-kW and 35-kW. Canister deposition plots are shown in Figure 3-17 and Figure 3-18 for the 35-kW cases. The results show a significant increase in canister deposition for both the vertical MAGNASTOR model and the horizontal HSM-15 model. For the vertical model most of the deposition takes place at the lid of the canister, as seen in the previous MAGNASTOR deposition model without turbulent dispersion. The horizontal canister has a significant increase in particle deposition with turbulent dispersion turned on and most of the deposition occurs along the top of the canister from 0 to 180 degrees radially along the canister.

These results are preliminary and need to be studied further, especially for the horizontal canister. Due to the significant increase in deposition for the horizontal model the authors recommend that the turbophoresis mechanism be studied further. The turbulent model, wall treatment model, and mesh resolution of the near wall cells all need to be studied further in the model. Since the flow is driven by natural convection and the temperature difference within the storage module, it is a complex interaction between the thermal and deposition models. It is not known if the turbulence model required for the thermal model is the same turbulence model needed to correctly capture all deposition mechanisms. The authors highly recommend additional future work to look at turbulence and the turbulent dispersion particle model, especially for a horizontal storage canister.

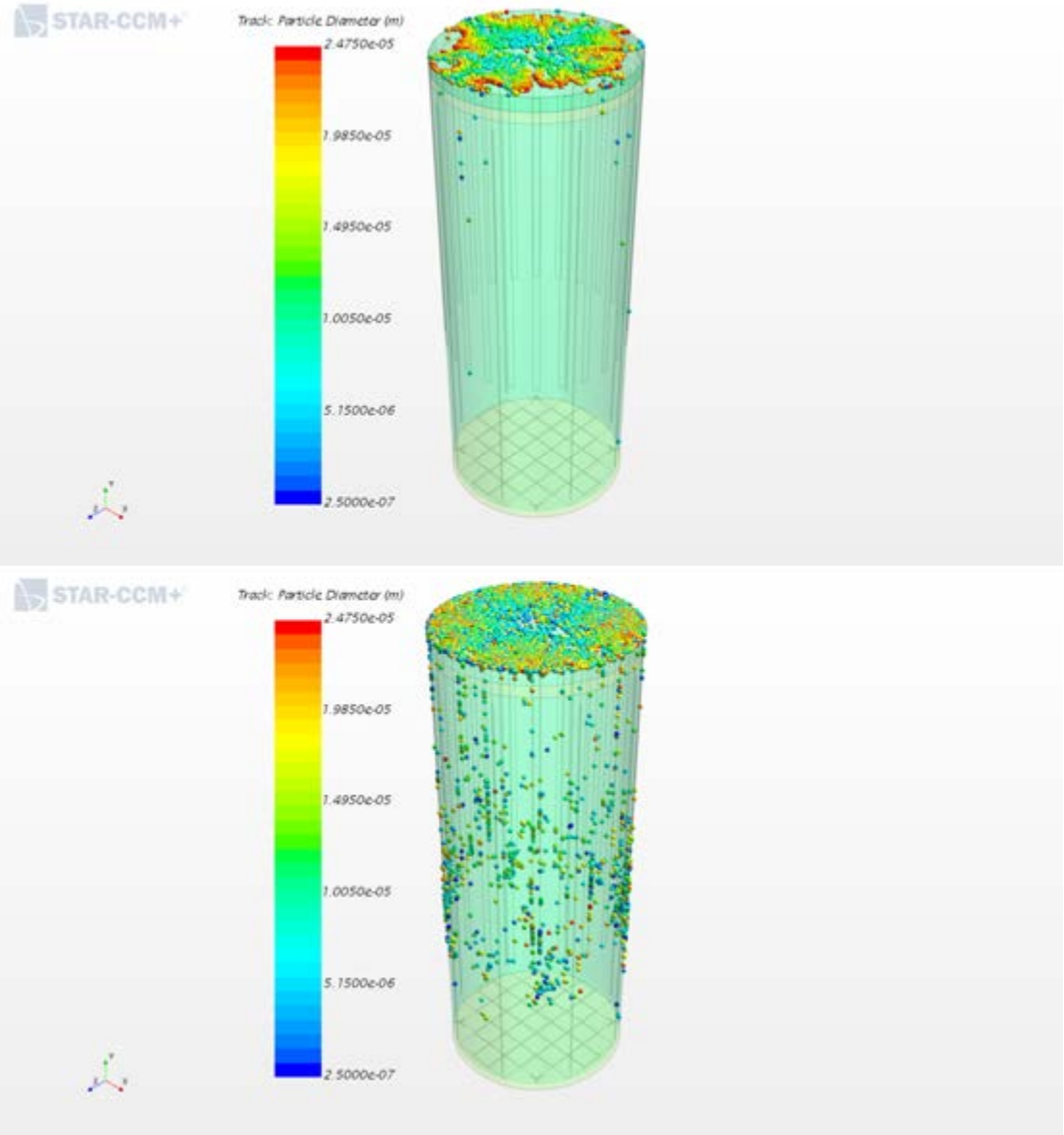

Figure 3-17. Canister deposition for vertical MAGNASTOR model with 35-kW heat load for no turbulent dispersion (top) and with turbulent dispersion (bottom).

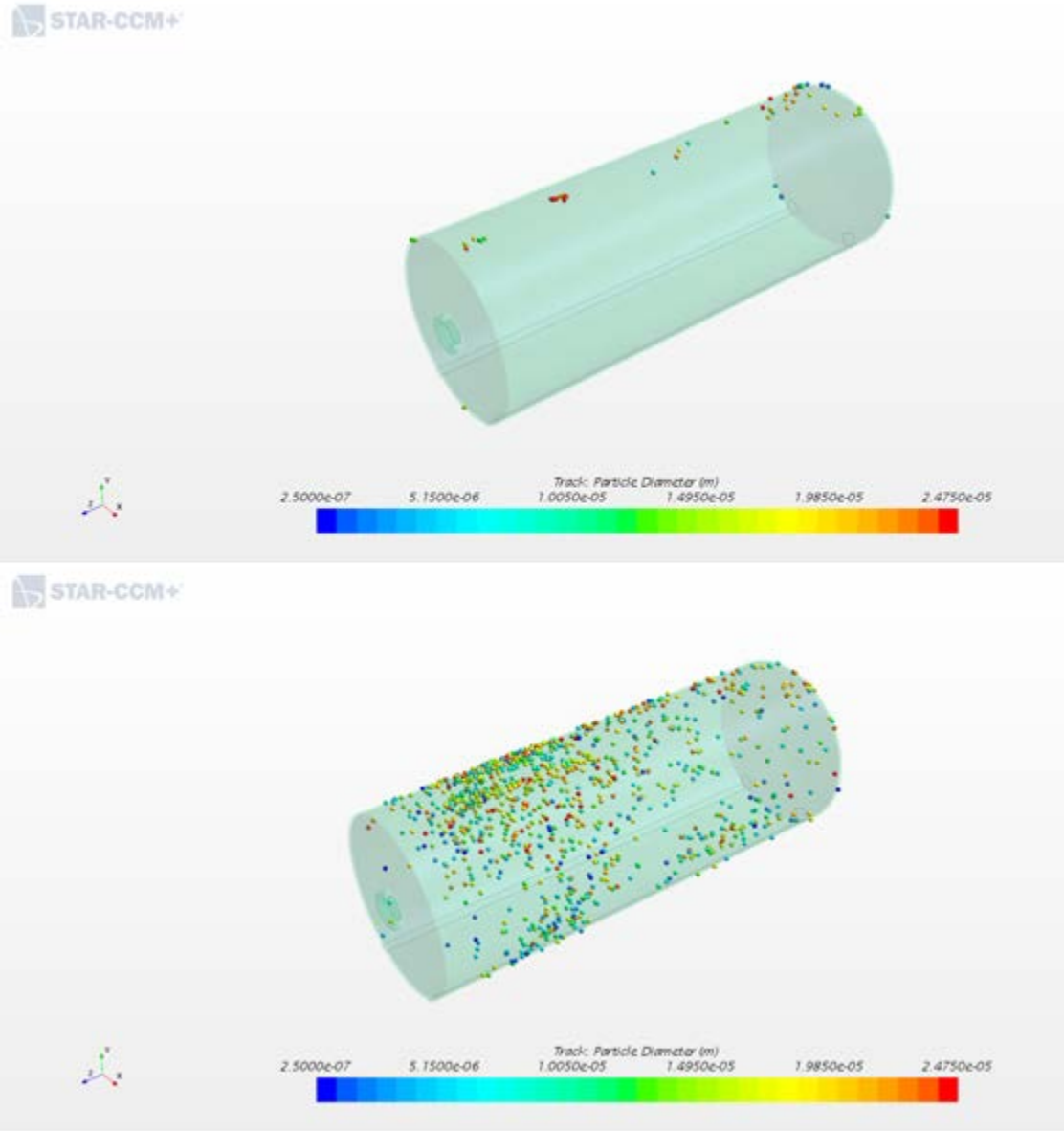

Figure 3-18. Canister deposition for horizontal HSM-15 model with 35-kW heat load for no turbulent dispersion (top) and with turbulent dispersion (bottom).

This page is intentionally left blank.

4. FUTURE WORK

The authors recommend the following future work to understand the CISCC deposition:

Experimental:

- Small Scale Validation - Small scale experimental data is needed to isolate specific particle deposition phenomena. Currently the existing body of literature is limited and not entirely applicable to the unique thermo-fluid environments relevant to SNF canister deposition. Experimental data would be used to benchmark models and to determine the most accurate and efficient ways to incorporate deposition phenomena into SNF canister deposition models.
- Large Scale Validation – Large scale validation testing will be necessary if SNF canister deposition models are to be used for SNF canister ageing management.

Modeling:

- Wind effects:
  - A standalone study concerning model development and best practices is needed.
  - A site wide wind effects model of an independent spent fuel storage installation ISFSI.
  - Transient wind effect modeling
- Latin hypercube sampling sensitivity study to look at the influence of various particle forces, particle distributions, temperatures, percent RH, etc.
- Develop an efficient transient model for running transient Brownian particle forces.
- Investigate alternative methods and equations for implementing Brownian motion in a steady state analysis.
- Determine run-to-run variability of a transient particle analysis.
- Continue development of multiphase models with particle size variability:
  - Run the multiphase evaporation model across various temperature and percent RH conditions.
  - Determine how to characterize deposition with evaporating particles.
  - Characterize multicomponent particle composition and update models.
- Continue development of multiphase fluid film model:
  - Create and run a validation model.
  - Develop an efficient transient model for running a fluid film model.
  - Integrate droplet film transition model.
  - Tie together condensation and evaporation of a fluid film surface and diffusiophoresis.
- Evaluate particle turbulent dispersion/turbophoresis within STAR-CCM+:
  - Validation case/model
  - Mesh GCI study
  - Turbulence model sensitivity study.
  - Boundary layer model sensitivity study.

This page is intentionally left blank.

5. CONCLUSION

FY 2020 deposition modeling status is presented herein; these efforts are ongoing and will continue into FY 2021.

The FY2020 modeling included the development of a wind effects model, which is the first step in developing a sitewide ISFSI model. The wind effects modeling determined deposition efficiency for the HSM-15 at four windspeeds at 2.5 m/s, 5 m/s, 15 m/s, and 26.5 m/s at directions varying 30 degrees from 0 degrees to 180 degrees. The HSM-15 was modeled with high and low heat loads (35kW and 5kW), and in all cases canister deposition efficiency was low.

Additional deposition mechanisms and particle phenomenon are under investigation, and initial work is demonstrated. This includes Brownian Motion, multiphase fluid modeling, particle size variability, diffusiophoresis, and turbophoresis. Additional work is necessary in these areas, with a focus on determining the relative importance of each phenomenon and developing modeling best practices.

Future work is discussed, with a focus on the need for additional experimental data and modeling studies.

This page is intentionally left blank.

6. REFERENCES

Davies JF, AE Haddrell, REH Miles, CR Bull, and JP Reid. 2012. “Bulk, Surface, and Gas-Phase Limited Water Transport in Aerosol.” *Journal of Physical Chemistry* A, 116 (45):10987−10998. https://pubs.acs.org/doi/pdf/10.1021/jp3086667.

Field A. 2017. *How can Brownian motion be modeled in STAR-CCM+*. Siemens Support Center, https://support.sw.siemens.com/knowledge-base/KB000015073_EN_US.

Jensen PJ, SR Suffield, CL Grant, CJ Spits, and JT Simmons. 2020. *Preliminary Deposition Modeling: For Determining the Deposition of Corrosive Contaminants on SNF Canisters.* PNNL-29620. Pacific Northwest National Laboratory, Richland, Washington.

Hsu SA, EA Meindl, and DB Gilhousen. 1994. “Determining the Power-Law Wind-Profile Exponent under Near-Neutral Stability Conditions at Sea.” Journal of Applied Meteorology, 33(6):757-765. https://www.jstor.org/stable/26186719.

United States Nuclear Regulatory Commission, “Continued Storage of Spent Nuclear Fuel," (2014)

United States Nuclear Regulatory Commission, “Potential Chloride-Induced Stress Corrosion Cracking of Austenitic Stainless Steel and Maintenance of Dry Cask Storage System Canisters," (2012).

Pilat MJ and A Prem. 1976. “Calculated particle collection efficiencies of single droplets including inertial impaction, brownian, diffusion, diffusiophoresis and thermophoresis.” *Atmospheric Environment*, 10:13-19. https://doi.org/10.1016/0004-6981(76)90253-5.

Siemens PLM Software. 2020. STAR-CCM+ 2020.1 (computer software). Siemens PLM Software, Plano, Texas.

Siemens. 2020. *External Aerodynamics with Simcenter STAR-CCM+ Best Practice Guidelines (2020.2).* Siemens Digital Industries Software, Plano, Texas.

Suffield, SR, JA Fort, HE Adkins, JM Cuta, BA Collins, and ER Siciliano. 2012. *Thermal Modeling of NUHOMS HSM-15 and HSM-1 Storage Modules at Calvert Cliffs Nuclear Power Station ISFSI*. PNNL-21788, Pacific Northwest National Laboratory, Richland, Washington.